Local proliferation maintains a stable pool of tissue-resident memory T cells following antiviral recall responses

Simone L. Park[1,4], Ali Zaid[1,4], Jyh Liang Hor[1], Susan N. Christo[1], Julia E. Prier[1], Brooke Davies[1], Yannick O. Alexandre[1], Julia L. Gregory[1], Tiffany A. Russell[2], Thomas Gebhardt[1], Francis R. Carbone[1], David C. Tscharke[2], William R. Heath[1,3], Scott N. Mueller[1,3,5] and Laura K. Mackay[1,3,5]

[1]Department of Microbiology and Immunology, The University of Melbourne, The Peter Doherty Institute for Infection and Immunity, Melbourne Victoria 3000, Australia

[2]John Curtin School of Medical Research, The Australian National University, Canberra, ACT 0200, Australia

[3]The Australian Research Council Centre of Excellence in Advanced Molecular Imaging, the University of Melbourne, Melbourne 3000, Australia

[4]These authors contributed equally to this work.

[5] These authors jointly directed this work.

Correspondence should be addressed to S.N.M. (smue@unimelb.edu.au) or L.K.M (lkmackay@unimelb.edu.au)

Running title: T_{RM} recall responses

Key words: Tissue-Resident Memory T cells, peripheral immunity, intravital imaging

While tissue-resident memory T (T_{RM}) cells play a critical role against infection, their fate following local pathogen reencounter is unknown. Here, we found that skin T_{RM} cells engaged virus infected cells, proliferated *in situ* in response to local antigen encounter and did not migrate out of the epidermis where they exclusively reside. As a consequence, secondary T_{RM} cells formed from pre-existing T_{RM} cells, as well as from precursors recruited from the circulation. Importantly, newly recruited antigen-specific or bystander T_{RM} cells were generated in the skin without displacement of the pre-existing T_{RM} cell pool. Thus, pre-existing skin T_{RM} populations are not displaced by subsequent infections, enabling multiple T_{RM} cell specificities to be stably maintained within the tissue.

Tissue-resident memory T (T_{RM}) cells are non-circulating lymphocytes that preferentially localize to sites of pathogen entry. T_{RM} cells are critical mediators of anti-pathogen immunity and are becoming recognized as key players in cancer, autoimmune and allergic pathologies[1, 2]. These cells exist in most organs and tissues in both humans and mice, and are found at high densities at sites of previous infection or inflammation[3, 4, 5]. T_{RM} cells are generated from precursors transiently present in the circulation, and are phenotypically distinct from circulating memory T cells (T_{CIRCM}), bearing a unique transcriptional profile that is acquired during differentiation in the tissue[6, 7, 8, 9].

The restricted anatomical localization and unique gene expression program enables T_{RM} cells to mediate local immunosurveillance and rapid protection against reinfection. Local antigen sensing by T_{RM} cells can also result in the enhanced recruitment of both adaptive and innate circulating cells to the site of T_{RM} cell activation[10, 11, 12]. However, surprisingly little is known regarding the fate of T_{RM} cells following secondary pathogen encounter. It is not known if T_{RM} cells persist into secondary memory after recall responses, or whether pre-existing T_{RM} cells are displaced by "new" T_{RM} cell populations generated by subsequent infections. It is also unclear whether reactivation of T_{RM} cells can lead to re-entry into the recirculating pool.

Skin T_{RM} cells persist in the epidermis, where they remain at the site of initial lodgment without diffusing through the tissue[13, 14]. Skin T_{RM} cells show minimal evidence of turnover in the steady-state[15], depend uniquely on fatty acid metabolism[16] and express molecules associated with inhibitory T cell function. Therefore, it might be expected that T_{RM} cells are terminally differentiated and unable to expand and survive following recall. Here, we examined the T_{RM} cell response to secondary viral infection utilizing experimental approaches that enabled the comparison of responses by T_{RM} and T_{CIRCM} cells. We utilized a model of herpes simplex virus type 1 (HSV) infection that infects the skin before entering the sensory ganglia, where it emerges via zositeriform spread as a band of lesions over the dermatome that is innervated by a single nerve[17]. T_{RM} cells in the tissue can block peripheral HSV replication indirectly by affecting neuronal infection[18]. To determine if skin-lodged T_{RM} cells can control HSV directly at the skin surface, we reasoned that protection would be confined to regions of skin that contained an area, or "patch" of embedded T_{RM} cells. We show that in response to secondary viral infection, T_{RM} cells mediate such local protection, engage virus-infected cells, remain constrained to their epidermal niche and proliferate *in situ*. Skin T_{RM} cells were maintained as a stable population after recall. Furthermore, we found

that pre-existing T_{RM} cells were not displaced by newly recruited T_{RM} populations, but instead they remained as a numerically stable population in the tissue.

Results

Skin T_{RM} cells mediate local immune protection

To understand how T_{RM} cells directly control virus infection at the point of pathogen entry, we *in vitro* activated congenically marked CD45.1$^+$ gBT-I transgenic CD8$^+$ T cells that are specific for the immunodominant determinant from HSV ($gB_{498-505}$) to generate effector T (T_{EFF}) cells. gBT-I T_{EFF} cells were transferred i.v. into C57BL/6 mice and were recruited into a patch of lower flank skin in a non-specific manner using the contact sensitizer DNFB[19]. This approach generates skin T_{RM} cells at frequencies similar to that of the $gB_{498-505}$-specific endogenous response induced by HSV infection but importantly, leaves the sensory ganglia unpopulated by T cells. CD45.1$^+$ gBT-I T_{RM} cells expressing the surface markers CD69 and CD103 were present in DNFB-treated skin, but not in untreated contralateral skin (**Supplementary Fig. 1a, b**). HSV was inoculated on the upper flank skin >1cm above the DNFB-treated patch containing gBT-I T_{RM} cells to induce HSV replication and infection of the sensory ganglia (**Supplementary Fig. 1c**). 6d after HSV infection, a band of herpetic lesions spread across the dermatome from the point of inoculation, but the DNFB-treated skin patch remained clear of disease (**Supplementary Fig. 1d**). Viral titers were reduced 4d and 6d after infection in DNFB-treated skin that contained gBT-I T_{RM} cells, compared to contralateral skin or to skin treated with DNFB but not transferred with gBT-I T cells (**Fig. 1a**). Thus, CD8$^+$ T_{RM} cells can control HSV infection in the skin in a very discrete and localized manner.

Density of skin T_{RM} cells influences local immune protection

Upon restimulation, T_{RM} cells may facilitate enhanced recruitment of memory T cells from the circulation[12]. We examined whether this was the case following recall of DNFB-lodged skin T_{RM} cells via HSV infection on the DNFB-untreated upper flank. We observed reduced recruitment of CD103$^-$ CD45.1$^+$ gBT-I T cells into DNFB-treated skin containing CD103$^+$ CD45.1$^+$ gBT-I T_{RM} cells 3-6d post-HSV infection, when compared to skin that did not contain gBT-I T_{RM} cells (**Fig. 1b**). This indicated that skin T_{RM} cells were dominating local virus protection, consistent with previous findings showing that T_{RM} cells can protect in the absence of T_{CIRCM} cells[20, 21, 22, 23]. To assess whether this protective response required an appropriate density of T_{RM} cells to mediate protection, we transferred increasing numbers of Thy1.1$^+$ gBT-I T_{EFF} cells into mice followed by DNFB-mediated skin lodgement. Mice were rested for >30d and injected i.p. with Thy1.1-specific antibody to deplete the Thy1.1$^+$ gBT-I

T_{CIRCM} cells without affecting skin T_{RM} cells[20]. Increasing the number of input Thy1.1$^+$ gBT-I T cells resulted in a concomitant increase in the number of Thy1.1$^+$ gBT-I T_{RM} cells in DNFB-treated skin (**Fig. 1c**), and induced a dose-dependent reduction in viral load 6d following HSV infection above the DNFB-treated skin patch (**Fig. 1d**). Thus, skin T_{RM} cells mediate protection from infection in a manner dependent on their local density in the tissue and independent of circulating T cells.

Antigen-specific T_{RM} cells exhibit dynamic responses to skin infection

To examine how skin T_{RM} cells mediate protection following infection, we transferred *in vitro* activated EGFP$^+$ gBT-I T cells into mice followed by DNFB-mediated skin lodgement. More than 30d following EGFP$^+$ gBT-I T cell transfer we imaged the DNFB-treated skin patch by intravital 2-photon microscopy (IV-2PM)[24]. EGFP$^+$ gBT-I T cells displayed a dendritic morphology, slow migration and were evenly distributed across the epidermal layer but absent from the dermis in a manner characteristic of skin T_{RM} cells[13] (**Fig. 2a**). To determine if skin T_{RM} cells could respond to antigen *in situ*, >30d following EGFP$^+$ gBT-I T cell transfer and DNFB treatment, we delivered antigen directly into the epidermis by mixing HSV-derived gB peptide with aqueous sorbolene cream and topically applying it to depilated skin[25]. Starting at 3h after gB peptide application we observed changes in the dendritic morphology of skin EGFP$^+$ gBT-I T_{RM} cells, which became more rounded with shorter dendrites, and displayed reduced motility (**Fig. 2b,c and Movie 1**). In contrast, application of non-specific ovalbumin (OVA) peptide did not alter the appearance or motility of skin EGFP$^+$ gBT-I T_{RM} cells (**Fig. 2b,c** and **Movie 1**), indicating that epidermal T_{RM} cells responded to cognate antigen *in situ*.

We next examined the localization and migration of T_{RM} cells in DNFB-treated lower flank skin 3-4d following infection of the DNFB-untreated upper flank skin with HSV-mCherry[26]. Following zosteriform spread, small epidermal foci of infected HSV-mCherry$^+$ cells were observed in DNFB-treated skin by 3.5d post-infection, and slow, but noticeable spreading of mCherry$^+$ HSV occurred over the 4h imaging period (**Supplementary Fig. 2a**). EGFP$^+$ gBT-I T cells clustered near HSV-mCherry$^+$ infected cells, while epidermal cells distal to virus foci remained evenly distributed (**Supplementary Fig. 2b**). This suggested local accumulation of EGFP$^+$ gBT-I T cells in response to the virus, but without the possibility of distinguishing between T_{RM} cells and T cells recruited from the circulation. We also observed highly motile EGFP$^+$ gBT-I T cells in the underlying dermis (**Fig. 2d and Movie 2**). EGFP$^+$

gBT-I T cells that engaged mCherry$^+$ HSV-infected cells showed reduced motility and more restricted migration around the virus foci compared with the EGFP$^+$ gBT-I T cells not recruited to foci of HSV-infected cells (**Fig. 2e, f**). Non-specific EGFP$^+$ OT-I T cells transferred to a second group of DNFB-treated mice as a control did not cluster in this manner following mCherry$^+$ HSV challenge (**Fig. 2d and Movie 3**). EGFP$^+$ OT-I T_{RM} cells also retained their dendritic morphology, motility and epidermal localization following mCherry$^+$ HSV challenge (**Fig. 2d and Movie 3**), suggesting that the changes in T_{RM} cell behavior we observed during viral recall depended on recognition of cognate antigen. To confirm this, we co-transferred equal numbers of activated EGFP$^+$ gBT-I T cells with lymphocytic choriomeningitis virus (LCMV)-specific DsRed$^+$ P14 T cells and treated mice with DNFB to generate skin T_{RM} of alternate specifities on the lower flank. 30d later, mice were challenged with CFP$^+$ HSV on the upper flank and DNFB-treated skin imaged by IV-2PM. EGFP$^+$ gBT-I T_{RM} cells clustered and dynamically engaged CFP$^+$ HSV-infected cells 3.5d following infection, while DsRed$^+$ P14 T cells did not (**Supplementary Fig. 2c**). Thus, local HSV infection drove dynamic responses by skin T_{RM} cells that were dependent on antigen-specific signals.

Skin T_{RM} cell responses are epidermally constrained during recall

We next asked whether epidermal T_{RM} cells could migrate towards foci of infected keratinocytes as well as into the underlying dermis. To distinguish between gBT-I T_{RM} cells and gBT-I T cells recruited from the circulation, we treated mice in which Thy1.1$^+$ EGFP$^+$ gBT-I T_{RM} cells had been lodged by DNFB treatment with Thy1.1 antibody, to selectively remove Thy1.1$^+$ gBT-I T_{CIRCM} cells. 10d after antibody treatment, mice were infected above the DNFB-treated skin with HSV-mCherry and imaged by IV-2PM 4d later. EGFP$^+$ gBT-I T_{RM} cells in the mCherry$^+$ virus foci adopted a rounded morphology and were more sessile than nearby EGFP$^+$ T_{RM} cells that were not in contact with virus-infected cells (**Fig. 3a, b and Movie 4**). Importantly, although we had observed highly motile dermal EGFP$^+$ gBT-I T cells in undepleted mice (**Fig 2d and Movie 2**), we did not observe EGFP$^+$ gBT-I T cells in the dermis of Thy1.1 antibody-treated mice (**Fig. 3c**), indicating that T_{RM} cells responding to challenge within the epidermis did not transit into the dermis.

Next, we directly compared the recall responses of DNFB-lodged T_{RM} cells with those mediated by memory T cells recruited from the circulation. To do this, we generated DNFB-recruited skin T_{RM} cells using gBT-I T cells expressing the photoconvertible protein Kaede,

which changes from green to red fluorescence upon exposure to violet light[27]. Mice were infected with HSV-CFP above DNFB-treated skin and 2d later the DNFB skin patch was photoconverted, resulting in Kaede-red$^+$ epidermal T_{RM} cells, whilst unconverted gBT-I T cells in the circulation remained Kaede-green$^+$. Following the spread of HSV to the lower skin flank on d3.5, both Kaede-red$^+$ and Kaede-green$^+$ gBT-I T cells accumulated around CFP$^+$ HSV foci (**Fig. 3d**). Kaede-red$^+$ gBT-I T cells that were distal to virus remained evenly distributed and localized to the epidermis, with a lower average velocity compared to the predominantly Kaede-green$^+$ gBT-I T cells in the dermis (**Fig. 3e**). To assess if T_{RM} cells migrated from skin to LN during the recall response, we next examined the distribution of photoconverted and unconverted gBT-I T cells in the skin and draining axillary lymph node (dLN) 4-5d after infection with HSV. The majority (91 ± 4.6%) of gBT-I T cells in the skin 4d after HSV infection were Kaede-red$^+$ (**Fig. 3f, g**), indicating that these were resident in the skin prior to viral spread. On d5 post-infection, a greater proportion (34 ± 25%) of Kaede-green$^+$ gBT-I T cells was observed in the skin (**Fig. 3g**), indicating recruitment of gBT-I T cells from the circulation. Notably, we could not detect Kaede-red$^+$ gBT-I T cells in the dLN at either time point after infection (**Fig. 3g**). Moreover, the Kaede-red$^+$ gBT-I T cells retained a CD103$^+$CD69$^+$ T_{RM} cell phenotype, distinct from that of Kaede-green$^+$ gBT-I T cells that were CD103$^-$CD69$^-$ (**Fig. 3h, i**). Together, these data indicate that skin T_{RM} cells responding to recall virus infection remained constrained to the epidermis and did not migrate into the dermis or local draining lymph nodes.

T_{RM} cells proliferate locally in response to antigenic challenge

Phenotypic flow cytometry analysis of gBT-I T_{RM} cells isolated from previously challenged skin >30d after HSV infection or DNFB treatment showed increased surface expression of multiple co-inhibitory molecules, including PD-1, Tim-3, LAG3, CD101, CD244, CTLA4 and ICOS in comparison with gBT-I T_{CIRCM} cells (**Supplementary Fig. 3a, b**). Because these inhibitory receptors are involved in the inhibition of T cell proliferation and effector functions[28], we tested whether skin T_{RM} cells could undergo significant numerical expansion upon challenge. As such, we generated mice with DNFB-lodged Thy1.1$^+$ gBT-I T_{RM} cells and treated them >30d later with Thy1.1 antibody to deplete gBT-I T_{CIRCM} cells or with PBS as control. Following infection with HSV above DNFB-treated skin, mice were treated i.p. with bromodeoxyuridine (BrdU) to assess the proliferative capacity of DNFB-lodged T_{RM} cells responding to HSV spread (**Supplementary Fig. 4a**). 7d post-HSV infection, a

population of circulating $CD103^-$ gBT-I T cells was detected in the DNFB-treated skin of PBS-treated control mice, whereas only $CD103^+$ T_{RM} cells were detected in DNFB-treated skin of Thy1.1 antibody-treated mice (**Fig. 4a**). Notably, a substantial proportion (36 ± 5.4 %) of $CD103^+$ gBT-I T_{RM} cells from the skin of Thy1.1-depleted mice had incorporated BrdU 7d post-infection (**Fig. 4b, c**). The proliferation marker Ki67 was also upregulated by skin gBT-I T_{RM} cells following infection (**Fig. 4b and Supplementary Fig. 4b**), indicating that skin T_{RM} cells proliferated *in situ* upon rechallenge. Ki67 was also upregulated by gBT-I T cells in the spleen of PBS-treated controls after HSV infection (**Supplementary Fig. 4c**). Divided $BrdU^+$ gBT-I T_{RM} cells in DNFB-treated skin of Thy1.1-depleted mice remained $CD103^+$ 7d post-HSV infection (**Supplementary Fig. 4d**), suggesting that T_{RM} cell proliferation expanded or maintained the epidermal T_{RM} cell pool and that T_{RM} cells did not give rise to $CD103^-$ T cells, nor lose CD103 expression upon stimulation. In a separate approach, we induced skin gBT-I T_{RM} cells from adoptively transferred $Thy1.1^+$ gBT-I naïve T (T_N) cells by e.c. skin infection with recombinant vaccinia virus (VV) expressing the HSV gB epitope (VV-gB) on the lower flank. After 30d mice were treated with Thy1.1 antibody to deplete $Thy1.1^+$ gBT-I T_{CIRCM} cells and >7d later infected with HSV above the primary VV infection site and subsequently treated with BrdU (**Supplementary Fig. 4a**). Increased BrdU incorporation by skin $Thy1.1^+$ gBT-I T_{RM} cells (33.3 ± 4.8%) was observed in comparison with uninfected mice (7.3 ± 2.7%), indicating virally primed T_{RM} cells also divide upon rechallenge (**Fig. 4d**). We also assessed the uptake of BrdU by gBT-I T_{RM} cells 2d after transcutaneous application of HSV-gB peptide (**Fig 4e**). T_{RM} cells induced by DNFB recruitment or local HSV infection showed similar proliferative responses (45 ± 15% and 42 ± 6.6% $BrdU^+$, respectively) in response to HSV-gB peptide application (**Supplementary Fig. 4e**). Finally, we tested whether skin gBT-I T_{RM} cell proliferation was antigen-specific by applying HSV-gB peptide or a non-specific OVA peptide to the skin of DNFB-treated mice administered BrdU, and observed that division of skin $Thy1.1^+$ gBT-I T_{RM} cells only occurred in response to cognate antigen (**Fig. 4f**). Together, these observations indicated that skin T_{RM} cells were not terminally differentiated and divided *in situ* in response to viral challenge.

However, we observed only a marginal increase in $Thy1.1^+$ gBT-I T_{RM} cell numbers in DNFB-treated skin between 3 and 14d after HSV infection above the DNFB patch compared to uninfected mice (**Supplementary Fig. 4f**). Amongst the rechallenged gBT-I T_{RM} cell population we observed an increase in the proportion of $annexinV^+$ (from 8.5 ± 0.7% to 18 ±

2.2%) and annexinV$^+$ PI$^+$ cells (from 7 ± 0.7% to 11 ± 0.9%) 7d post HSV infection compared to DNFB-lodged gBT-I T_{RM} cells at steady state (**Supplementary Fig. 4f and g**), indicative of increased apoptosis of T_{RM} cells upon recall in addition to heightened proliferation. In all, these data indicate that T_{RM} cells can be maintained by local proliferation during secondary infections, without the requirement for replenishment from the circulating T cell pool.

Circulating T cells form T_{RM} cells without displacing pre-existing T_{RM} cells

Next, we examined whether antigen-specific memory T cells in the circulation were recruited to inflamed skin and developed into T_{RM} cells after secondary challenge. We also asked how these incoming cells impacted on populations of pre-existing T_{RM} cells in the skin. To this end, we performed antibody-mediated enrichment of CD44$^+$CD45.1$^+$ gBT-I T_{CIRCM} cells isolated from spleens of mice that were previously infected with HSV and transferred them into Thy1.1antibody-treated recipient mice possessing DNFB-lodged Thy1.1$^+$ gBT-I skin T_{RM} cells. 2d following CD45.1$^+$ gBT-I T_{CIRCM} cell transfer, recipient mice were infected with HSV above DNFB-treated skin to restimulate both skin T_{RM} cells and adoptively transferred T_{CIRCM} cells (**Supplementary Fig. 5a**). CD45.1$^+$ gBT-I T_{CIRCM} cells were detected in DNFB-treated skin alongside Thy1.1$^+$ gBT-I T_{RM} cells and persisted for at least 30d after HSV infection (**Fig. 5a, b**). CD45.1$^+$ gBT-I T_{CIRCM} cells infiltrating the skin upregulated both CD69 and CD103 (**Fig. 5c**), indicative of *de novo* T_{RM} cell formation from circulating memory precursors. Importantly, stable numbers of Thy1.1$^+$ gBT-I T_{RM} cells were maintained in the DNFB-treated skin before and after HSV challenge, irrespective of CD45.1$^+$ gBT-I T_{CIRCM} transfer (**Fig. 5b**), indicating that the pre-existing skin T_{RM} cell population was not displaced by subsequent T_{RM} cell generation. Together, these findings indicate that both local maintenance of pre-existing T_{RM} cells and *de novo* differentiation of restimulated T_{CIRCM} cells into T_{RM} cells contribute independently to maintenance or expansion of the T_{RM} cell pool upon secondary infection.

We then sought to determine whether CD8$^+$ T_{EFF} cells of an unrelated specificity would give rise to T_{RM} cells in HSV-infected skin containing pre-existing T_{RM} cells. Mice with DNFB-lodged non-HSV-specific Thy1.1$^+$ P14 skin T_{RM} cells were depleted of Thy1.1$^+$ P14 T_{CIRCM} cells by administration of Thy1.1 antibody and infected with HSV above the DNFB patch >7d later. Mice were adoptively transferred with *in vitro*-activated CD45.1$^+$ OT-I T_{EFF} cells and examined after 30d (**Supplementary Fig. 5b**). HSV infection resulted in non-HSV-

specific CD45.1$^+$ OT-I T_{EFF} cell recruitment into DNFB-treated skin (**Fig. 5d, e**), and these bystander CD45.1$^+$ OT-I T_{EFF} cells had converted to a CD69$^+$CD103$^+$ T_{RM} cell phenotype (**Fig. 5f**). The number of pre-existing Thy1.1$^+$ P14 skin T_{RM} cells was not affected by CD45.1$^+$ OT-I T_{EFF} cell transfer despite *de novo* OT-I T_{RM} cell formation (**Fig. 5e**).

Because the presence of local antigen in the tissue can influence the formation of T_{RM} cells[29, 30, 31], we next examined the recall of T_{RM} cells induced by direct skin infection with a virus rather than DNFB recruitment. Mice were transferred with naïve Thy1.1$^+$ gBT-I (T_N) cells and infected on the lower flank skin with VV-gB to generate a population of Thy1.1$^+$ gBT-I T_{RM} cells and Thy1.1$^+$ gBT-I T_{CIRCM} cells were subsequently depleted by Thy1.1 antibody administration. More than 30d following VV-gB infection and >7d following T_{CIRCM} depletion, mice were challenged with HSV above the initial VV-gB scarification site and transferred with *in vitro* activated CD45.1$^+$ non-specific OT-I T_{EFF} cells (**Supplementary Fig. 5c**). Both Thy1.1$^+$ gBT-I T_{RM} cells generated in response to VV-gB infection and bystander CD45.1$^+$ OT-I T_{RM} cells were detected in skin at the previously infected VV-gB site >30d after HSV challenge (Fig. 5g-i). The number of Thy1.1$^+$ gBT-I T_{RM} cells in VV-gB challenged skin was not altered after HSV infection, and unchanged by the transfer of bystander OT-I T_{EFF} cells, despite induction of substantial OT-I T_{RM} cells after HSV infection (**Fig. 5h**), suggesting that virally induced T_{RM} cells are also stably maintained upon reinfection. Further, to examine recall responses to HSV in the absence of antibody-mediated protection, B cell-deficient *Igmh*(μMT)$^{-/-}$_mice adoptively transferred with Thy1.1$^+$ gBT-I T_N cells were infected with HSV on the lower flank and treated with Thy1.1 antibody >30d post-infection to induce T_{CIRCM} depletion. 10d following T_{CIRCM} depletion, mice were re-challenged on the upper flank with HSV and transferred *in vitro* activated OT-I CD45.1 T_{EFF} cells (**Supplementary Fig. 5d**). Thy1.1$^+$ gBT-I T_{RM} cells generated by the primary HSV infection were detected in post-lesional skin >30d following HSV rechallenge (**Supplementary Fig. 5e**). Previously infected skin also contained CD45.1$^+$ OT-I T_{EFF} that had converted into CD69$^+$CD103$^+$ T_{RM} cells, without impacting the numbers of Thy1.1$^+$ gBT-I T_{RM} cells (**Supplementary Fig. 5e**). Combined, these results show that pre-existing and incoming T_{RM} cell populations of identical or different specificities can be maintained and established concomitantly, and do not outcompete one another in the context of local infection.

New T_{RM} cells minimally dislodge of pre-existing T_{RM} cells

To determine whether a maximal capacity for T_{RM} cell generation exists within the skin, we transferred increasing numbers of CD45.1$^+$ gBT-I T_{EFF} cells into mice and induced T_{RM} cell lodgement in the skin using DNFB. Although increased T cell input in the range of 1-100×10^6 gBT-I T_{EFF} cells resulted in increasing numbers of splenic gBT-I T cells (**Fig. 6a**), the number of skin gBT-I T_{RM} cells plateaued following an input of 50-100×10^6 gBT-I T cells (**Fig. 6a**), indicating a limited number of T_{RM} cells could be generated in the skin, at least during a single inflammatory response. To test whether subsequent responses could add to the T_{RM} cell pool, we transferred CD45.1$^+$ gBT-I T_N cells into mice containing DNFB-induced skin EGFP$^+$ OT-I T_{RM} cells. After >30d, mice were subjected to a prime-boost immunization with i.v. transferred gB-pulsed DC followed by s.c. and i.n. infection with recombinant influenza viruses, which results in widespread generation of skin T_{RM} cells[31], and a separate cohort of mice were left untreated (**Supplementary Fig. 6a**). More than 30d after influenza virus infection, a pool of newly generated ('new') CD45.1$^+$ gBT-I T_{RM} cells of a different TCR specificity was detected in DNFB-treated skin that also contained 'old' EGFP$^+$ OT-I T_{RM} cells (**Fig. 6b**). Importantly, generation of new T_{RM} cells by multiple route prime-boost immunization allowed us to test if dislodgement of pre-existing T_{RM} cells occurred in the absence of perturbation to the skin tissue itself. We detected minimal numerical decay of DNFB-induced 'old' skin EGFP$^+$ OT-I T_{RM} cells in prime-boost immunized mice in comparison to control mice that were not subjected to prime-boost immunization (**Fig. 6b**), indicating that *de novo* formation of T_{RM} cells with different specificities occurs without displacing pre-existing T_{RM} cells in the tissue. Moreover, when DNFB-treated mice possessing 'old' CD45.1$^+$ gBT-I T_{RM} cells were adoptively transferred with EGFP$^+$ OT-I T_N cells, and 'new' T_{RM} cell formation was induced via multiple skin immunizations (e.c. infection with VV-OVA contralateral to DNFB-treated skin followed by secondary VV-OVA infection at an unrelated skin site) (**Supplementary Fig 6b**), the number of pre-existing CD45.1$^+$ gBT-I skin T_{RM} cells remained constant in comparison with non-immunized mice (**Fig 6c**). Collectively, these findings highlight the exceptional stability of skin T_{RM} cell populations following rechallenge.

Discussion

Here, we found that T_{RM} cells respond in an antigen-specific manner, proliferate and survive following local restimulation, and are not dislodged by newly generated T_{RM} cells . This has important implications for understanding how immune memory is maintained within peripheral tissues. We show that T_{RM} cell-mediated protection is directly linked to the density of T_{RM} cells in the skin. This finding has been predicted by mathematical models that showed an inverse correlation of the number of $CD8^+$ T cells in the genital mucosa after HSV reactivation with the severity of disease[32]. We observed that T_{RM} cells interacting with virus-infected cells decelerated and were restimulated, whilst T_{RM} cells in nearby uninfected epidermis continued to exhibit random migration. Our imaging did not reveal any obvious attraction of T_{RM} cells towards virally infected cells, suggesting that T_{RM} cells need to be in the right place at the right time to protect against infection. Consequently, it may take hours to days for epidermal T_{RM} cells to chance upon infected cells, highlighting the importance of T_{RM} cell density for protection. We found that T_{RM} cells could protect against local infection independently of T_{CIRCM} cells, although the mechanism through which T_{RM} cells execute protection is unclear. It has been shown that T_{RM} cells can directly kill infected cell targets[33]. Whilst we observed skin T_{RM} cells engaging virally infected cells, we were unable to regularly document killing of infected targets by $CD8^+$ T cells in the skin (data not shown). It is possible that density of T_{RM} cells inversely regulates the recruitment of T cells from the circulation, as near-sterile immunity induced by local T_{RM} cells might negate the need to recruit large numbers of T_{CIRCM} cells and reduce inflammation.

T_{RM} cells proliferated in response to antigen, yet numbers of secondary T_{RM} cells in the absence of T_{CIRCM} cells did not markedly increase. Skin T_{RM} cell populations appeared to maintain stability by balancing cell death with proliferation, as we observed increased annexinV staining of skin T_{RM} cells upon viral recall. Restimulated T_{RM} cells did not exit the epidermis even after proliferation. T_{RM} cells survive poorly when removed from tissues[33] (and our unpublished observations), potentially limiting their relocation to other tissues. Collectively, our results indicate T_{RM} cells, at least in the skin, are a durable and autonomous population. It will however be important to ascertain whether T_{RM} cells in other organs are similarly tissue-restricted upon reactivation, particularly in tissues such as the lungs, where local T_{RM} cell maintenance relies on constant replenishment from circulating cells[34].

411 We show that T_{CIRCM} and T_{EFF} cells are recruited into the skin upon pathogen reencounter
412 where some convert to T_{RM} cells, thereby adding to the T_{RM} cell pool. Our findings suggest
413 that T_{RM} cells can be maintained in tissues subject to repeated infections, with unrelated
414 infections unlikely to substantially dislodge T_{RM} cells already in the tissue. Such knowledge
415 is of clinical relevance to help shape vaccine strategies that might induce diverse T_{RM} cells to
416 protect against multiple diseases. Nonetheless, under conditions where T_{RM} cells of certain
417 specificities are undesirable, such as psoriasis in the skin[35, 36], replacing unwelcome T_{RM} cells
418 with desired T_{RM} populations may be a challenge.
419
420
421

Acknowledgements

We thank C. Jones, G. Davey, M. Damtsis and N. Zamudio for technical assistance. S.L.P. was supported by the Elizabeth and Vernon Puzey Postgraduate Scholarship. T.G. was supported by a fellowship from the Sylvia and Charles Viertel Charitable Foundation. This work was supported by the National Health and Medical Research Council of Australia and the Australian Research Council.

Author contributions

S.L.P., A.Z., J.L.H., S.N.C., J.E.P., B.D., Y.O.A., J.L.G., S.N.M. and L.K.M. performed experiments and analyzed data; T.A.R. and D.C.T. provided reagents; S.L.P., A.Z., T.G. F.R.C., W.R.H., S.N.M. and L.K.M. contributed to experimental design. S.L.P., S.N.M. and L.K.M. prepared the manuscript; S.N.M. and L.K.M. led the research program.

Competing financial interests statement

The authors declare no competing financial interests.

Methods

Mice and infections. C57BL/6, gBT-I, gBT-I.xB6.SJL-PtprcaPep3b/BoyJ (gBT-I.CD45.1), gBT-I.Thy1.1, gBT-I.ubiquitin-EGFP (gBT-I.EGFP), gBT-I.EGFP.Thy1.1, gBT-I.Kaede, OT-I.EGFP, P14.DsRed, P14.Thy1.1, OT-I.CD45.1 and *Igmh*(μMT)$^{-/-}$_ mice were bred in the Department of Microbiology and Immunology, The University of Melbourne. gBT-I mice encode a transgene for a T-cell receptor recognizing the HSV-1 glycoprotein B (gB)-derived epitope $gB_{498\text{-}505}$[37]. Animal experiments were approved by The University of Melbourne Animal Ethics Committee. Epicutaneous (e.c.) infection by scarification was done using 1×10^6 plaque forming units HSV-1 KOS, HSV-1 pCmC (HSV-mCherry)[26] or HSVgDUL47ΔYFP (HSV-CFP)[38] as described[39], or with recombinant vaccinia viruses expressing $gB_{498\text{-}505}$ (VV-gB)[40] or ovalbumin (VV-OVA)[41]. Strains of recombinant influenza virus expressing gB used were WSN-gB and X31-gB (H1N1) and were administered s.c. or i.n. as described[31]. Viral titers were determined in homogenized skin by performing PFU assays as previously described[15].

Adoptive T cell transfer and DNFB treatment Transgenic gBT-I, OT-I or P14 $CD8^+$ T cells were activated *in vitro* by incubation for 4-5d with $gB_{498\text{-}505}$ (SSIEFARL), OVA (SIINFEKL) or gp33 (KAVYNFATM) peptide-pulsed splenocytes in the presence of recombinant human IL-2 (25U/mL, PeproTech), as described previously[15]. Except where indicated, 2-10 x 10^6 effector gBT-I or OT-I T cells were adoptively transferred i.v. Mice were shaved and depilated before the application of 15μl DNFB in acetone/oil (4:1) to a 1.5 cm^2 area of skin on the day of T cell transfer. Alternatively, 5×10^4 – 1×10^6 naïve gBT-I or OT-I T cells were transferred i.v. prior to infection. For adoptive transfer of $CD8^+$ memory T cells, cells were enriched from spleens of HSV-immune mice >30d post-infection by staining cell suspensions with anti-CD4 (GK1.5), anti-CD11b (M1/70), anti-F4/80 (F4/80), anti-erythrocyte (TER-119), anti-I-A/I-E (M5114) monocolonal antibodies and then incubating cells with goat-anti-rat IgG-coupled magnetic beads (Qiagen) prior to removal of bead-bound cells.

Flow cytometry. Cells were isolated from the spleen and lymph nodes (LN) by grinding organs through a metal mesh to create single cell suspensions. T cells were isolated from the skin as previously described[19]. Briefly, skin was incubated in dispase (2.5mg/mL, Roche)

solution at 37°C for 90 min and the epidermis separated from the dermis. The dermis was chopped and incubated in collagenase type 3 (3 mg/mL, Worthington) at 37°C for 30 min and the epidermis placed in trypsin/EDTA (Sigma) and incubated at 37°C for 30 min. Cells were stained with antibodies and their expression of phenotypic markers determined using a BD Fortessa (BD Biosciences) or BD FACSCanto II (BD Biosciences) and analyzed using Flowjo (Treestar). Antibodies used were: anti-mouse CD45.1 (A20), CD8α (53-6.7), Vα2 (B20.1), CD69 (H1.2F3), CD16/CD32 (2.4G2), and anti-BrdU (B24) from BD Biosciences; anti-mouse CD45.1 (A20), CD3e (eBio500A2), CD8α (53-6.7), CD69 (H1.2F3), CD103 (2E7) Ki67 (20Raj1) CD101 (Moushi101), CD244 (eBio244F4), CTLA4 (UC10-4B9), LAG3 (e9B7W), PD-1 (J43) and TIM-3 (8B.2C12) from eBioscience; anti-mouse CD45.2 (104), CD103 (2E7), CD8α (53-6.7), CD103 (2E7) Thy1.1 (OX-7) and ICOS (C398.4A), from Biolegend. Live cells were discriminated using a Fixable Live/Dead stain (Life Technologies or Biolegend) or by propidium iodide staining. AnnexinV staining was determined using a BD AnnexinV FITC staining kit according to the manufacturer's instructions. Cells were enumerated by adding a known number of calibration particles (BD Biosciences) to each sample before analysis.

Intravital two photon microscopy. Mice were anaesthetized with isoflurane (Cenvet; 2.5% for induction, 1-1.5% for maintenance, vaporized at 80:20 mixture of O_2 and air), and were shaved on the left flank and hair depilated for flank skin imaging as described elsewhere[42]. Briefly, two incisions (~15mm apart) were made longitudinally along the left flank, cutting through the dermis, and the peritoneum separated by cutting away the connective tissues underneath the skin. A 18mm-wide x 1mm thick stainless steel platform was inserted under the exposed dermis, which was glued to the platform with vetbond tissue adhesive (3M). The edges of the skin were lined with vacuum grease (Dow Corning), upon which a glass coverslip was placed. Imaging was performed with an upright LSM710 NLO multiphoton microscope (Carl Zeiss) with a 20×/1.0 NA water immersion objective enclosed in an environmental chamber that was maintained at 35°C with heated air. Fluorescence excitation was provided by a Chameleon Vision II Ti:sapphire laser (Coherent) with dispersion correction and fluorescence emission detected using external non-descanned photomultiplier tubes. EGFP, and second-harmonic generation were excited at 920 nm, mCherry at 960-980 nm. Kaede-green was excited at 800nm and Kaede-red at 900nm. For four-dimensional data sets, three-dimensional stacks were captured every 1min for at least 30min. Raw imaging

data were then processed with Imaris 8 (Bitplane) and movies generated in Imaris and composed in After Effects (Adobe).

Intravital imaging analysis. To distinguish gBT-I T cells based on contact with virus-infected keratinocytes, tracks were generated using Imaris Spot function, and mCherry positive virus-infected cells were rendered as a three-dimensional surface. Tracks were computed using a custom-modified version of the script 'Surface to Spot Distance' through an XT/Matlab interface (Mathworks). To segregate T cells in contact with virus, we used the center of each gBT-I T cell and defined contact as cells remaining within 10μm of rendered virus ($mCherry^+$ or CFP^+) for at least 5min. Statistical values for mean track speed and mean track displacement length were extracted from Imaris software. Statistical significance was determined by Mann-Whitney U-Test.

Depletion of circulating gBT-I Thy1.1 T cells. > 20d following activated gBT-I Thy1.1 cell transfer and DNFB treatment, mice were injected i.p. 1-3 times with 0.5-4μg anti-mouse/rat Thy1.1 mAb (α-Thy1.1, clone HIS57; eBioscience) in PBS. Control mice received PBS alone.

In vivo **photoconversion of gBT-I Kaede T_{RM} cells.** Mice containing gBT-I Kaede T_{RM} cells were anesthetized, shaved and depilated and infected with HSV-mCherry. At 2d post-infection, mice were exposed under a 410nm spot lamp (Dymax Bluewave LED; UV Pacific) to 100mJ/cm^2 of violet light for 6min. Light emitted through an 8mm diameter fiber optic guide was mounted at a distance of 4.17cm directly above the DNFB patch, while areas around the patch were covered with a double layer of aluminium foil to prevent distal photoconversion. Mice were then imaged by IV-2PM from 94h post-infection.

Transcutaneous delivery of gB and OVA peptide. 50μg of MHC-I-restricted HSV $gB_{498-505}$ (SSIEFARL) or ovalbumin (SIINFEKL) peptides (Genscript) were mixed with 100mg Sorbolene cream and thoroughly mixed by successive vortexing and short-pulse centrifugation. Mice containing DNFB-lodged T_{RM} cells were anesthetized, shaved and depilated, and the peptide/sorbolene mixture was applied directly atop the DNFB patch. The peptide/cream mixture was contained above the skin region using a bandage consisting of an adhesive film (OpSite Flexigrid, Smith & Nephew) and surgical tape (Micropore Tape, 3M). For intravital imaging experiments, the mixture was allowed to absorb through the skin for 3h

prior to removal of the bandage. For flow cytometry experiments, peptide/sorbolene mixture was applied once per day for 2d and mice bandaged for 24h following each application.

***In vivo* Bromodeoxyuridine (BrdU) treatment.** Mice were injected i.p. with 2mg BrdU per day, with treatment commencing on the day of transcutaneous peptide application or 0-2d post infection. BrdU incorporation was measured using a BrdU Flow Kit (BD Biosciences) or FoxP3 staining kit (eBioscience) and where indicated the proportion $BrdU^+$ cells was determined by the Overton method of population comparison[42] (FlowJo, Treestar) using skin gBT-I T cells from an untreated mouse as the control population.

Generation and transfer of bone marrow-derived dendritic cells. Dendritic cells were differentiated by culturing C57BL/6 bone marrow cells in the presence of 20ng/mL GM-CSF and IL-4 for 7d. Dendritic cells were matured overnight in the presence of 150ng/mL LPS then pulsed with 1μg/mL $gB_{498\text{-}505}$ (SSIEFARL) peptide for 45min before transfer of 2.5×10^5 cells i.v. to recipients.

Statistics and reproducibility. Two-tailed Mann Whitney *U*-tests, one way ANOVA with Tukey's multiple comparisons test or Kruskal Wallis tests with Dunn's multiple comparison test were used where indicated. All proportional numerical values provided in the text are written as the mean ± standard error of the mean. All statistical analyses were performed in Prism 7.0 (Graphpad). All experiments were performed at least two times with similar results obtained.

Data availability. Publically available source data was not used in this study. Data supporting the findings of this study are available from the corresponding author upon request.

Figure Legends

Figure 1. Anti-viral protection by skin T_{RM} cells correlates with T_{RM} cell density. (**a**) Skin HSV titers 4d and 6d after HSV infection of the upper flank in mice receiving *in vitro* activated gBT-I T cells and treated with DNFB on the lower left flank. DNFB-treated skin (DNFB + T_{RM}) or untreated skin from the right (contralateral) flank were analysed, as well as skin from mice treated with DNFB but not receiving gBT-I T cells (DNFB). Data are representative of 2 experiments with n= 4 or 6 mice per group per experiment. **p= 0.0004, **p= 0.005, ****p< 0.0001, one-way ANOVA with Tukey's multiple comparisons test. (**b**) Enumeration of $CD103^-$ gBT-I T cells in DNFB-treated or contralateral skin following HSV infection. Data are representative of 2 experiments with n= 3 or 5 mice per group per experiment. (**c**) Mice received 0-20 x 10^6 $Thy1.1^+$ gBT-I T_{EFF} cells, were treated with DNFB and depleted of $Thy1.1^+$ T_{CIRCM} cells >30d later. Shown is the number of $CD103^+$ T_{RM} in DNFB-treated skin >7d post Thy1.1 antibody treatment. Data are pooled from 2 experiments with n= 5 or 6 mice per group. (**d**) DNFB-treated skin HSV-titres in cohorts described in **c** 6d after HSV infection. Data are pooled from 2 experiments with n= 8 or 10 mice per group. ***p= 0.005 in **c**, ***p< 0.0001 in **d**, Kruskal Wallis test with Dunn's post-test. Bars represent the mean.

Figure 2. T_{RM} cells respond in an antigen-specific manner upon HSV challenge. **(a)** IV-2PM image of $EGFP^+$ gBT-I skin T_{RM} cells >30d post DNFB treatment. **(b)** IV-2PM images of $EGFP^+$ skin T_{RM} cells 3h post-gB or OVA peptide application. Scale bars; 20μm. Data in **a** and **b** are representative of 2 experiments with n= 5 or 6 mice per experiment. **(c)** Sphericity and velocity of skin $EGFP^+$ gBT-I T_{RM} cells 3h after gB or OVA peptide application. Data are pooled from 2 experiments with n= 5 or 6 mice per experiment. ****p< 0.0001, two-tailed Mann Whitney U-test. **(d)** Maximum intensity projection images acquired 92-114h after HSV-mCherry infection across x, y and z dimensions of skin containing DNFB-lodged $EGFP^+$ gBT-I or OT-I T cells. Scale bar; 60μm (left panel), 75μm (right panel). **(e)** Plots showing tracks of $EGFP^+$ gBT-I T cell migration in the skin 94h after HSV-mCherry infection in cells contacting $HSV\text{-}mCherry^+$ cells. **(f)** Velocity and track displacement length measurements of $EGFP^+$ gBT-I T cells contacting $mCherry^+$ virus-infected cells. Data in e and f are pooled from 5 mice from 1 of 4 representative experiments. *p= 0.0137, ****p< 0.0001, two-tailed Mann Whitney U-test. SHG, second harmonic generation (dermal collagen). Bars represent the mean.

Figure 3. Skin T_{RM} cells remain localized to the epidermis upon virus rechallenge. (**a**) IV-2PM image of $EGFP^+$ $Thy1.1^+$ T_{RM} cells entering HSV-$mCherry^+$ virus foci in DNFB-treated skin of T_{CIRCM} depleted mice 4d post-infection. Representative of 7 mice from 2 experiments. Scale bar; 30 μm. (**b**) Sphericity and velocity of $EGFP^+$ gBT-I Thy1.1 T_{RM} cells in cells contacting $mCherry^+$ cells 4d after HSV-mCherry infection. ****p< 0.0001, two-tailed Mann Whitney U-test. (**c**) Percentage of $EGFP^+$ $Thy1.1^+$ gBT-I T_{RM} cells localizing to the epidermis of DNFB-treated skin 4d after HSV-mCherry infection. Error bars represent mean ± SEM. Data in **b** and **c** are pooled from 2 experiments with n= 14 movies from 7 mice. (**d**) IV-2PM image of $Kaede^+$ gBT-I T_{RM} cells in DNFB-treated skin 3.5d after HSV-CFP infection above the DNFB patch and 2d after violet light exposure. Scale bar; 100 μm. (**e**) Velocity of Kaede-$green^+$ (unconverted) and Kaede-red^+ (converted) gBT-I T cells in DNFB-treated skin 3.5d post HSV-CFP infection and 2d after violet light exposure. ****p< 0.0001 two-tailed Mann Whitney U-test. Data are representative of 3 experiments with n = 3 mice per experiment in **d** and **e**. (**f-i**) Flow cytometry of $Kaede^+$ gBT-I T cell fluorescence phenotype in DNFB-treated skin and draining axillary LN (dLN) 4-5d post-HSV infection and 2d after violet light exposure. (**f, g**) Proportion of converted or unconverted $Kaede^+$ gBT-I T cells localizing to skin or dLN . (**h, i**) Expression of CD69 and CD103 amongst converted and unconverted $Kaede^+$ gBT-I T cells. Data are representative of 2 experiments with n= 6 mice per experiment. Error bars represent mean ± SEM. Bars represent the mean.

Figure 4. T_{RM} cells proliferate following antigenic challenge. (**a**) CD69 and CD103 expression by skin $Thy1.1^+$ gBT-I T_{RM} cells 7d post-infection in Thy1.1 antibody or PBS (control)-treated cohorts. (**b**) Representative BrdU and Ki67 staining on $CD103^+$ $Thy1.1^+$ gBT-I T_{RM} cells 7d after HSV challenge**.** Data in **a** and **b** are representative of 2 experiments with n = 3 or 4 mice per group. (**c**) Proportion of DNFB-lodged skin $CD103^+$ gBT-I T_{RM} cells incorporating BrdU in > 7d post-HSV infection or in non-infected mice, determined by the Overton method of population comparison. Data are pooled from 2 experiments with 6 or 8 mice per group. **p= 0.0022, **p= 0.0047, two-tailed Mann Whitney U-test. **(d)** Proportion of VV-gB lodged skin $CD103^+$ $Thy1.1^+$ gBT-I T_{RM} cells incorporating BrdU >7d post-HSV infection or in non-infected mice. Data are pooled from 2 experiments with 6 mice per group. **p= 0.0043, two-tailed Mann Whitney U-test. (**e**) Representative BrdU and Ki67 staining on $CD103^+$ $Thy1.1^+$ gBT-I T_{RM} cells 2d after HSV-gB peptide application. Data are representative of 2 experiments with n= 3 or 4 mice per group. **(f**) Proportion of skin $CD103^+$

Thy1.1$^+$ gBT-I T_{RM} cells incorporating BrdU 2d after topical HSV-gB or OVA peptide application determined by the Overton method of population comparison. Data are pooled from 2 independent experiments with n= 5 or 7 mice per group. **p= 0.0043, two-tailed Mann Whitney U-test. Bars represent the mean.

Figure 5. T_{CIRCM} cells and bystander T_{EFF} cells generate *de novo* T_{RM} cells following viral challenge. (**a**) Frequency of Thy1.1$^+$ gBT-I (DNFB-lodged) and CD45.1$^+$ gBT-I (T_{CIRCM} derived) T cells in DNFB-treated skin >30d post-HSV infection. Data are representative of 2 experiments with n= 3 or 5 mice per group. **(b)** Number of Thy1.1$^+$ gBT-I and CD45.1$^+$ gBT-I T_{RM} cells and **(c)** their CD69 and CD103 expression in DNFB-treated skin >30d post-HSV infection. Data are pooled from 2 experiments with n= 6 or 10 mice per group. ***p= 0.0002, two-tailed Mann Whitney test. **(d)** Frequency of Thy1.1$^+$ P14 (DNFB-lodged) and CD45.1$^+$ OT-I (T_{EFF} derived) T cells in DNFB-treated skin >30d post-HSV infection. Data are representative of 2 experiments with n= 4 or 5 mice per group. **(e)** Number of Thy1.1$^+$ P14 and CD45.1$^+$ OT-I T_{RM} cells and **(f)** their CD69 and CD103 expression in DNFB-treated skin >30d post-HSV infection. Data are pooled from 2 experiments with n= 9 mice per group. (**g**) Frequency of Thy1.1$^+$ gBT-I (VV-gB lodged) and CD45.1$^+$ OT-I (T_{EFF} derived) T cells in VV-gB challenged skin >30d post-HSV infection. Data are representative of 2 experiments with n= 4 mice per group. (**h**) Number of Thy1.1$^+$ gBT-I and CD45.1$^+$ OT-I T_{RM} cells and (**i**) their CD69 and CD103 expression in VV-gB challenged skin >30d post-HSV infection. Data are pooled from 2 experiments with n= 8 mice per group. ***p = 0.0002, two-tailed Mann Whitney U-test. Bars represent the mean.

Figure 6. *De novo* T_{RM} cell generation does not displace pre-existing T_{RM} cells in skin. **(a)** Mice were seeded with 1-100 x 10^6 CD45.1$^+$ gBT-I T_{EFF} cells and treated with DNFB. Shown is the number of gBT-I T cells in the spleen and CD103$^+$ T_{RM} cells in DNFB-treated skin >30d post-treatment. Data are pooled from 2 experiments with n= 6 or 7 mice per group. *p= 0.0262, n.s; not significant, two-tailed Mann Whitney test. **(b)** Number of 'old' (DNFB-lodged) EGFP$^+$ OT-I T_{RM} cells (generated from 50×10^6 input EGFP$^+$ OT-I T_{EFF} cells) and 'new' prime-boosted CD45.1$^+$ gBT-I T cells in DNFB-treated skin of flu-immunized mice >30d following final immunization, or in non-immunized mice. Data are pooled from 2 experiments with n= 18 or 25 mice per group. N.s.; not significant, Kruskal-Wallis test with Dunn's multiple comparisons. (**e**) Number of DNFB-lodged CD45.1$^+$ gBT-I T_{RM} cells and VV-OVA primed EGFP$^+$ OT-I T_{RM} cells in DNFB-treated skin >25d following final

673 contralateral VV-OVA immunization or in non-immunized mice. Data are pooled from 2
674 experiments with n= 9 or 10 mice. n.s., not significant; ** p = 0.0098, n.s., not significant,
675 Kruskal Wallis test with Dunn's multiple comparisons. Bars represent the mean.
676
677
678

References

1. Mueller, S.N. & Mackay, L.K. Tissue-resident memory T cells: local specialists in immune defence. *Nat. Rev. Immunol.* **16**, 79-89 (2016).

2. Park, C.O. & Kupper, T.S. The emerging role of resident memory T cells in protective immunity and inflammatory disease. *Nat. Med.* **21**, 688-697 (2015).

3. Casey, K.A. *et al.* Antigen-Independent Differentiation and Maintenance of Effector-like Resident Memory T Cells in Tissues. *J. Immunol.* **188**, 4866-4875 (2012).

4. Steinert, E.M. *et al.* Quantifying Memory CD8 T Cells Reveals Regionalization of Immunosurveillance. *Cell* **161**, 737-749 (2015).

5. Sathaliyawala, T. *et al.* Distribution and compartmentalization of human circulating and tissue-resident memory T cell subsets. *Immunity* **38**, 187-197 (2013).

6. Mackay, L.K. *et al.* The developmental pathway for CD103(+)CD8(+) tissue-resident memory T cells of skin. *Nat. immunol.* 14, 1294-1301 (2013).

7. Mackay, L.K. *et al.* Hobit and Blimp1 instruct a universal transcriptional program of tissue residency in lymphocytes. *Science* **352**, 459-463 (2016).

8. Wakim, L.M. *et al.* The molecular signature of tissue resident memory CD8 T cells isolated from the brain. *J. Immunol.* **189**, 3462-3471 (2012).

9. Hombrink, P. *et al.* Programs for the persistence, vigilance and control of human CD8+ lung-resident memory T cells. *Nat. Immunol.* **17**, 1467-1478 (2016).

10. Ariotti, S. *et al.* T cell memory. Skin-resident memory CD8(+) T cells trigger a state of tissue-wide pathogen alert. *Science* **346**, 101-105 (2014).

11. Schenkel, J.M. *et al.* T cell memory. Resident memory CD8 T cells trigger protective innate and adaptive immune responses. *Science* **346**, 98-101 (2014).

12. Schenkel, J.M., Fraser, K.A., Vezys, V. & Masopust, D. Sensing and alarm function of resident memory CD8(+) T cells. *Nat. Immunol.* **14**, 509-513 (2013).

13. Zaid, A. *et al.* Persistence of skin-resident memory T cells within an epidermal niche. *Proc. Natl. Acad. Sci. USA.* **111**, 5307-5312 (2014).

14. Ariotti, S. *et al.* Tissue-resident memory CD8+ T cells continuously patrol skin epithelia to quickly recognize local antigen. *Proc. Natl. Acad. Sci. USA.* **109**, 19739-19744 (2012).

15. Gebhardt, T. *et al.* Memory T cells in nonlymphoid tissue that provide enhanced local immunity during infection with herpes simplex virus. *Nat Immunol* **10**, 524-530 (2009).

16. Pan, Y. *et al.* Survival of tissue-resident memory T cells requires exogenous lipid uptake and metabolism. *Nature* **543**, 252-256 (2017).

17. Simmons, A. & Nash, A.A. Zosteriform spread of herpes simplex virus as a model of recrudescence and its use to investigate the role of immune cells in prevention of recurrent disease. *J. Virol.* **52**, 816-821 (1984).

18. Shin, H. & Iwasaki, A. A vaccine strategy that protects against genital herpes by establishing local memory T cells. *Nature* **491**, 463-467 (2012).

19. Mackay, L.K. *et al.* Long-lived epithelial immunity by tissue-resident memory T (TRM) cells in the absence of persisting local antigen presentation. *Proc. Natl. Acad. Sci. USA.* **109**, 7037-7042 (2012).

20. Mackay, L.K. *et al.* T-box Transcription Factors Combine with the Cytokines TGF-beta and IL-15 to Control Tissue-Resident Memory T Cell Fate. *Immunity* **43**, 1101-1111 (2015).

21. Jiang, X. *et al.* Skin infection generates non-migratory memory CD8+ T(RM) cells providing global skin immunity. *Nature* **483**, 227-231 (2012).

22. Wu, T. *et al.* Lung-resident memory CD8 T cells (TRM) are indispensable for optimal cross-protection against pulmonary virus infection. *J. Leukoc. Biol.* **95**, 215-224 (2014).

23. Zens, K.D., Chen, J.K. & Farber, D.L. Vaccine-generated lung tissue-resident memory T cells provide heterosubtypic protection to influenza infection. *JCI Insight* **1** (2016).

24. Gebhardt, T. *et al.* Different patterns of peripheral migration by memory CD4+ and CD8+ T cells. *Nature* **477**, 216-219 (2011).

25. Zaid, A. *et al.* Chemokine Receptor-Dependent Control of Skin Tissue-Resident Memory T Cell Formation. *J. Immunol.* **111**, 5307-5312 (2017).

26. Russell, T.A., Stefanovic, T. & Tscharke, D.C. Engineering herpes simplex viruses by infection-transfection methods including recombination site targeting by CRISPR/Cas9 nucleases. *J. Virol. Methods* **213**, 18-25 (2015).

27. Tomura, M. *et al.* Monitoring cellular movement in vivo with photoconvertible fluorescence protein Kaede transgenic mice. *Proc. Natl. Acad. Sci. USA.* **105**, 10871-10876 (2008).

28. Attanasio, J. & Wherry, E.J. Costimulatory and Coinhibitory Receptor Pathways in Infectious Disease. *Immunity* **44**, 1052-1068 (2016).

29. Khan, T.N., Mooster, J.L., Kilgore, A.M., Osborn, J.F. & Nolz, J.C. Local antigen in nonlymphoid tissue promotes resident memory CD8+ T cell formation during viral infection. *J. Exp. Med.* **213**, 951-966 (2016).

30. Muschaweckh, A. *et al.* Antigen-dependent competition shapes the local repertoire of tissue-resident memory CD8+ T cells. *J. Exp. Med.* **213**, 3075-3086 (2016).

31. Davies, B. *et al.* Cutting Edge: Tissue-Resident Memory T Cells Generated by Multiple Immunizations or Localized Deposition Provide Enhanced Immunity. *J. Immunol.* **198**, 2233-2237 (2017).

32. Schiffer, J.T. *et al.* Mucosal host immune response predicts the severity and duration of herpes simplex virus-2 genital tract shedding episodes. *Proc. Natl. Acad. Sci. USA.* **107**, 18973-18978 (2010).

33. Wakim, L.M., Woodward-Davis, A. & Bevan, M.J. Memory T cells persisting within the brain after local infection show functional adaptations to their tissue of residence. *Proc. Natl. Acad. Sci. USA.* **107**, 17872-17879 (2010).

34. Slütter, B. *et al.* Dynamics of influenza-induced lung-resident memory T cells underlie waning heterosubtypic immunity. *Sci. Immunol.* **2**, 2-11 (2017).

35. Cheuk, S. *et al.* CD49a Expression Defines Tissue-Resident CD8+ T Cells Poised for Cytotoxic Function in Human Skin. *Immunity* **46**, 287-300 (2017).

36. Clark, R.A. Skin-resident T cells: the ups and downs of on site immunity. *J. Invest. Derm.* **130**, 362-370 (2010).

37. Mueller, S.N., Heath, W., McLain, J.D., Carbone, F.R. & Jones, C.M. Characterization of two TCR transgenic mouse lines specific for herpes simplex virus. *Immunol. Cell Biol.* **80**, 156-163 (2002).

38. Macleod, B.L. *et al.* Distinct APC subtypes drive spatially segregated CD4+ and CD8+ T-cell effector activity during skin infection with HSV-1. *PLoS Pathog* **10**, e1004303 (2014).

39. van Lint, A. *et al.* Herpes simplex virus-specific CD8+ T cells can clear established lytic infections from skin and nerves and can partially limit the early spread of virus after cutaneous inoculation. *J. Immunol.* **172**, 392-397 (2004).

40. Blaney, J.E., Jr. *et al.* Immunization with a single major histocompatibility complex class I-restricted cytotoxic T-lymphocyte recognition epitope of herpes simplex virus type 2 confers protective immunity. *J Virol.* **72**, 9567-9574 (1998).

41. Restifo, N.P. *et al.* Antigen processing in vivo and the elicitation of primary CTL responses. *J. Immunol.* **154**, 4414-4422 (1995).

42. Overton, W.R. Modified histogram subtraction technique for analysis of flow cytometry data. *Cytometry* **9**, 619-626 (1988).

Figure 1

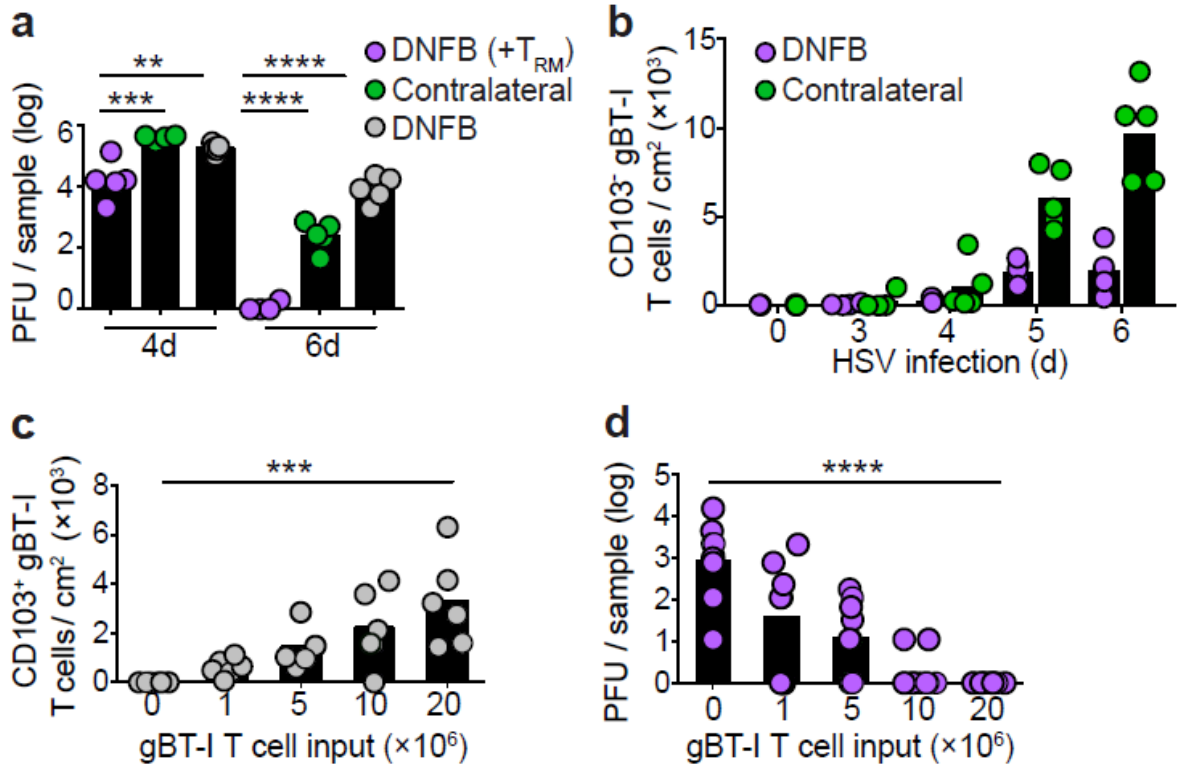
a
PFU / sample (log)
DNFB (+T_RM)
Contralateral
DNFB
**
***
****
****
4d
6d
b
CD103- gBT-I T cells / cm² (×10³)
DNFB
Contralateral
HSV infection (d)
c
CD103+ gBT-I T cells / cm² (×10³)
***
gBT-I T cell input (×10⁶)
d
PFU / sample (log)
****
gBT-I T cell input (×10⁶)

Figure 2

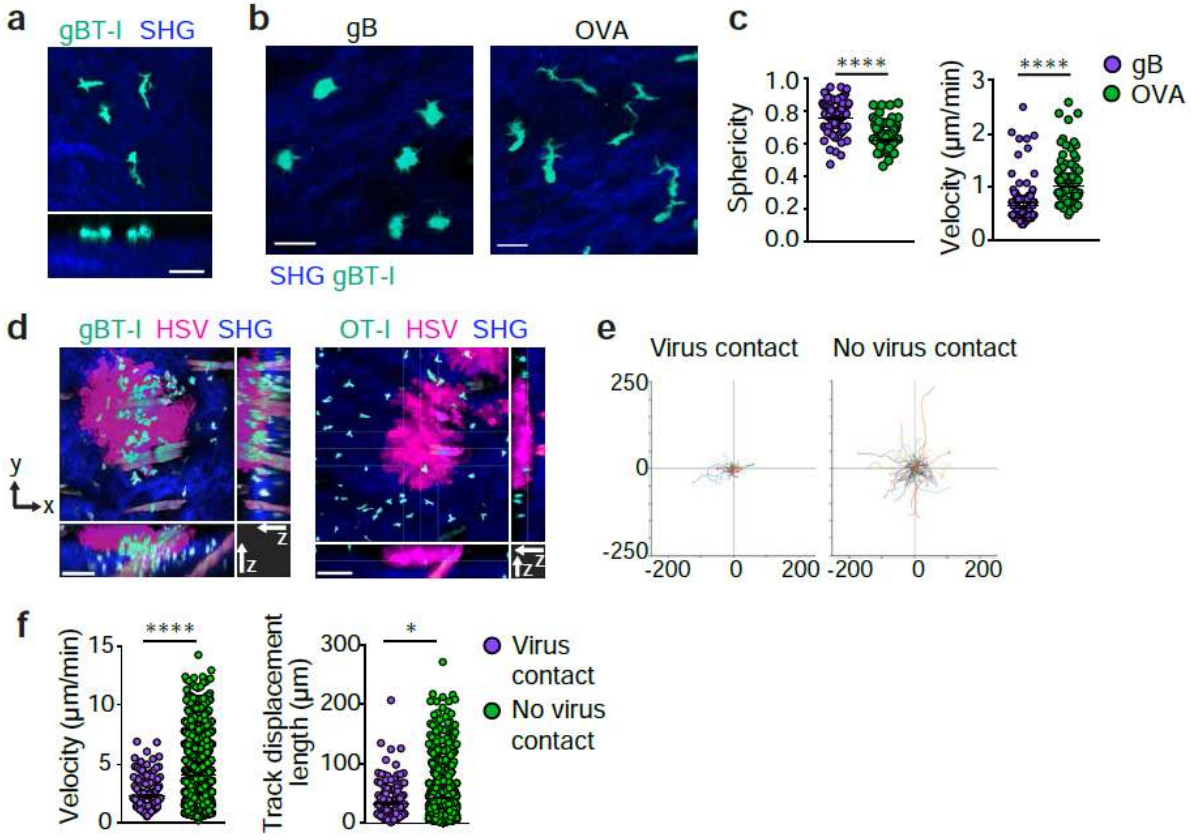
a
gBT-I SHG
b
gB
OVA
SHG gBT-I
c
Sphericity
1.0
0.8
0.6
0.4
0.2
0.0
****
Velocity (µm/min)
3
2
1
0
****
gB
OVA
d
gBT-I HSV SHG
OT-I HSV SHG
y
x
z
e
Virus contact
No virus contact
250
0
-250
-200
0
200
f
Velocity (µm/min)
15
10
5
0
****
Track displacement length (µm)
300
200
100
0
*
Virus contact
No virus contact

Figure 3

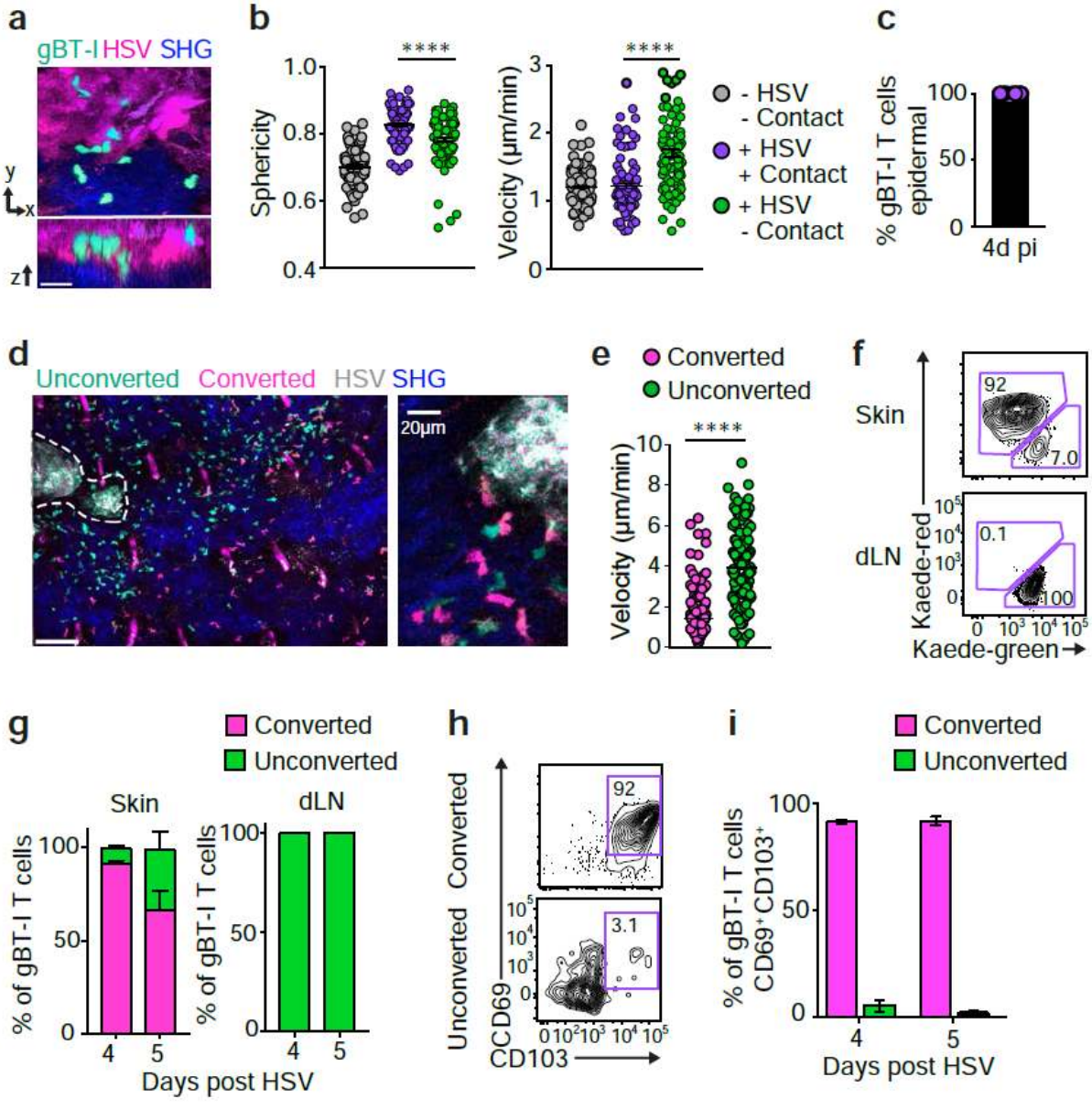
a
gBT-I HSV SHG
y
x
z
b
Sphericity
1.0
0.8
0.6
0.4
****
Velocity (μm/min)
3
2
1
0
****
- HSV
- Contact
+ HSV
+ Contact
+ HSV
- Contact
c
% gBT-I T cells epidermal
100
50
0
4d pi
d
Unconverted Converted HSV SHG
20μm
e
Converted
Unconverted
Velocity (μm/min)
10
8
6
4
2
0
****
f
Skin
dLN
92
7.0
0.1
100
Kaede-red
Kaede-green
g
Converted
Unconverted
Skin
dLN
% of gBT-I T cells
100
50
0
4
5
Days post HSV
h
Converted
Unconverted
92
3.1
CD69
CD103
i
Converted
Unconverted
% of gBT-I T cells CD69+CD103+
100
50
0
4
5
Days post HSV

Figure 4

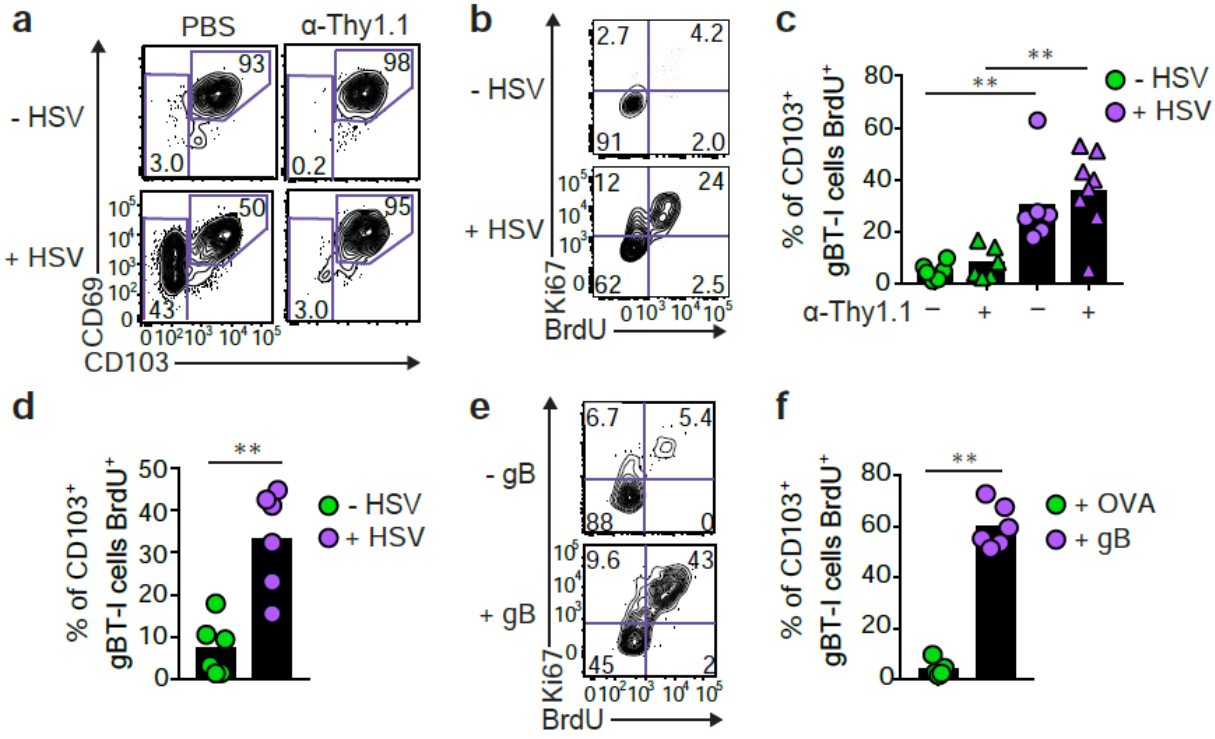
a
PBS
α-Thy1.1
- HSV
+ HSV
93
98
3.0
0.2
50
95
43
3.0
CD69
CD103
b
- HSV
+ HSV
2.7
4.2
91
2.0
12
24
62
2.5
Ki67
BrdU
c
% of CD103+ gBT-I cells BrdU+
- HSV
+ HSV
α-Thy1.1
**
**
d
% of CD103+ gBT-I cells BrdU+
**
- HSV
+ HSV
e
- gB
+ gB
6.7
5.4
88
0
9.6
43
45
2
Ki67
BrdU
f
% of CD103+ gBT-I cells BrdU+
**
+ OVA
+ gB

Figure 5

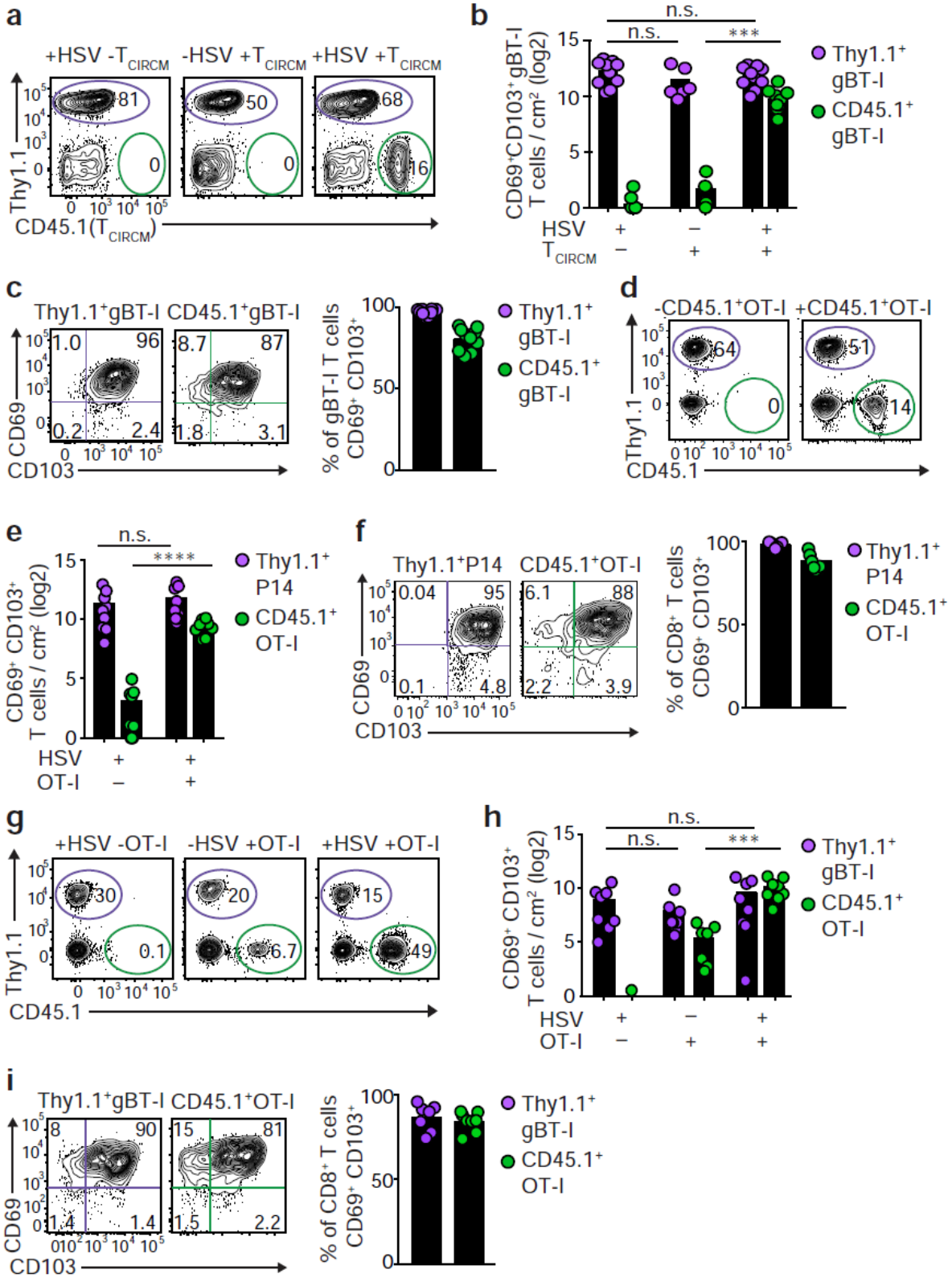
a
+HSV -T CIRCM
-HSV +T CIRCM
+HSV +T CIRCM
Thy1.1
CD45.1(T CIRCM)
81
0
50
0
68
16
b
n.s.
n.s.
***
CD69+CD103+gBT-I T cells / cm² (log2)
HSV
T CIRCM
Thy1.1+ gBT-I
CD45.1+ gBT-I
c
Thy1.1+gBT-I
CD45.1+gBT-I
CD69
CD103
1.0
96
0.2
2.4
8.7
87
1.8
3.1
% of gBT-I T cells CD69+ CD103+
Thy1.1+ gBT-I
CD45.1+ gBT-I
d
-CD45.1+OT-I
+CD45.1+OT-I
Thy1.1
CD45.1
64
0
51
14
e
n.s.
****
CD69+ CD103+ T cells / cm² (log2)
HSV
OT-I
Thy1.1+ P14
CD45.1+ OT-I
f
Thy1.1+P14
CD45.1+OT-I
CD69
CD103
0.04
95
0.1
4.8
6.1
88
2.2
3.9
% of CD8+ T cells CD69+ CD103+
Thy1.1+ P14
CD45.1+ OT-I
g
+HSV -OT-I
-HSV +OT-I
+HSV +OT-I
Thy1.1
CD45.1
30
0.1
20
6.7
15
49
h
n.s.
n.s.
***
CD69+ CD103+ T cells / cm² (log2)
HSV
OT-I
Thy1.1+ gBT-I
CD45.1+ OT-I
i
Thy1.1+gBT-I
CD45.1+OT-I
CD69
CD103
8
90
1.4
1.4
15
81
1.5
2.2
% of CD8+ T cells CD69+ CD103+
Thy1.1+ gBT-I
CD45.1+ OT-I

Figure 6

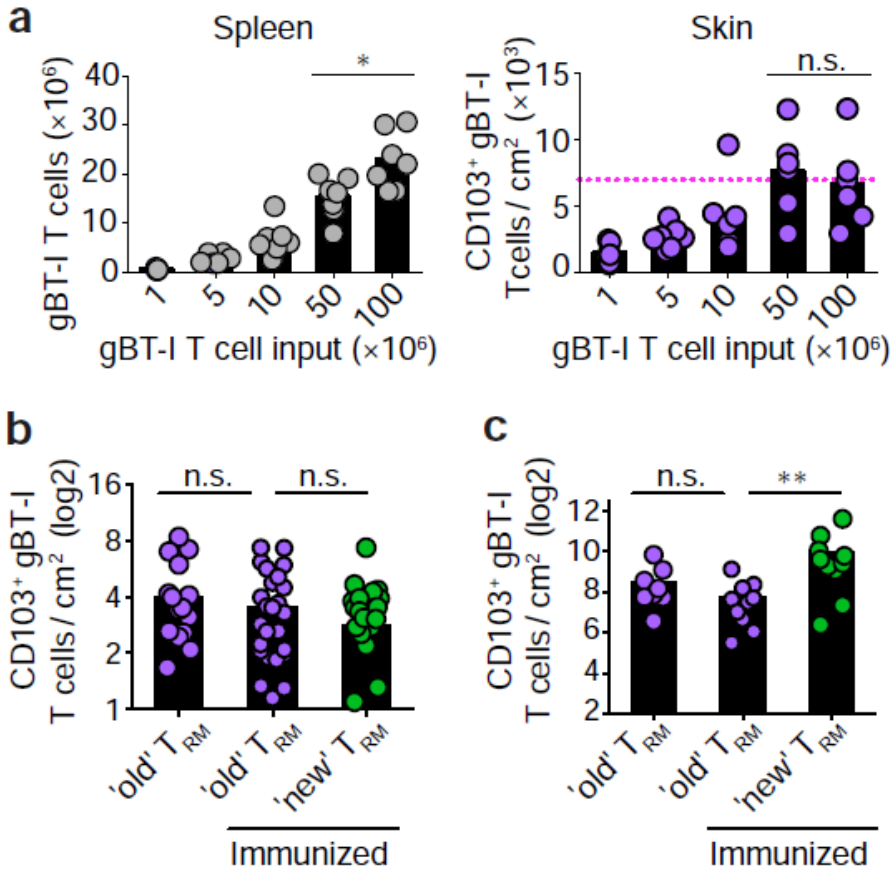
a
Spleen
Skin
gBT-I T cells (×10⁶)
CD103⁺ gBT-I Tcells / cm² (×10³)
gBT-I T cell input (×10⁶)
gBT-I T cell input (×10⁶)
*
n.s.
b
c
CD103⁺ gBT-I T cells / cm² (log2)
n.s.
n.s.
**
'old' T RM
'old' T RM
'new' T RM
Immunized
Immunized